Buffer structure optimization of the photoacoustic cell for trace gas detection*

CAI Yang (蔡洋)[1], **Norhana Arsad**[2], **LI Min** (黎敏)[1]**, and **WANG Yao** (王尧)[1]

1. Department of Physics, Wuhan University of Technology, Wuhan 430070, China

2. Department of Electric, Electronics & System Engineering, Faculty of Engineering & Built Environment, Universiti Kebangsaan Malaysia, Selangor 43600, Malaysia

(Received 25 January 2013)

The equivalent four-pole network model is used to simulate one-dimension longitudinal acoustic resonator with different buffer diameters and lengths, aiming to reach a theoretic model which is able to estimate the optimal buffer geometry. In experiments, the buffer volumes are decreased gradually by filling a set of aluminum rings with different inner diameters and lengths into the buffers to get the desired dimensions. The experimental results show that the average deviation of 1.1% is obtained between the experimental results and the theoretical simulation at the buffer length of 30 mm. Experiments show that the minimum background signal occurs when the buffer length is equal to a quarter of the acoustic wavelength (λ/4). The amplitude of the photoacoustic signal is barely influenced when $d_{buf}>3d_{res}$. Considering that oversize of photoacoustic cell needs more measuring gas and more material, the buffer diameter can be deduced to $d_{buf}\approx 3d_{res}$. Therefore, smaller photoacoustic cell is desirable.

Document code: A **Article ID:** 1673-1905(2013)03-0233-5

DOI 10.1007/s11801-013-3017-3

Photoacoustic spectroscopy (PAS) for trace gas detection technique finds applications in many fields, including environmental pollutants monitoring[1], medicine diagnostics[2], electrical power system[3,4] and so on. Based on the generation of an acoustic wave in the gas excited by a modulated diode laser with a wavelength corresponding to an absorption line of the gas species[5], and detecting with a highly sensitive microphone fixed on the photoacoustic cell[6], PAS has a very high sensitivity up to part per trillion (ppt) in trace gas detection[7].

The photoacoustic signal depends considerably on the geometry of the photoacoustic cell. Acoustical resonances enable highly sensitive analyses with low detection limits, thus most published papers used a resonant cell to conduct the PAS experiment. An optimum design of photoacoustic cell plays a vital role in achieving high photoacoustic response. As an important part of the photoacoustic cell, buffer has significant influence on the sensitivity and signal-to-noise ratio. Although the performances of different geometric photoacoustic cells have been compared in the past, discussions are rarely found on the optimization of the buffer. L. C. Aamodt[8] presented their works majorly on the size consideration of the resonant cell rather than the buffers. Simona Cris-tescu[9] emphasized the influence of different buffer radii on the sensitivity, but the experimental results were not enough to support the theoretical results. To obtain the optimal size of the buffer volume, F. G. C. Bijnen[10] tried to modify the dimension of one of the buffers to reach an optimal conclusion. Mohammed A. Gondal[11] tested different geometries of the photoacoustic cell, buffer and buffer gas to achieve low detection concentration of NO, but no quantitative estimation model on buffer geometry was given. M. Wolff[12] proposed an "hourglass cell" with an irregular buffer geometry, to achieve a stable signal increasing from 32% to 36% compared with the well-established H cell, which is too hard to be put into mass production.

In this paper, we work to reach a theoretic model which is able to estimate the optimal buffer geometry using electric circuit analogy called equivalent four-pole network model. We design an adjustable photoacoustic cell whose buffer dimensions can be modified, and demonstrate the validity of the simulation results. The experimental results and the deviation between the experimental and simulation results are given. Discussion and conclusion of the optimum buffer volume to realize a high sensitivity and signal-to-noise ratio of the photoacoustic cell are presented.

During the photoacoustic signal generation in the gas cell, several types of energy transformations occur, such

* This work has been supported by the National Natural Science Foundation of China (No.61177076), and the Fundamental Research Funds for the Central Universities (No.2012-Ia-020).

** E-mail: min.zoe@gmail.com

as photon energy transforming to heat and kinetic energy. These photoacoustic processes and parameters can be described by a series of discrete complex acoustic impedances and admittances of every element of the gas cell[13]. A simple electric circuit model, transmission line model[13] has been set up to simplify the calculation, where electric elements, such as resistances, capacitances, inductances, conductance, and current or voltage sources, are used as analogy concepts of the photoacoustic processes in an electric system. For example, resistance R, inductance L and capacitance C mean the viscous losses, stored kinetic energy and potential energy, respectively, and the source means the absorbed light power always described by a current or voltage source. Bernegger S. and Sigrist M. W.[14] reported an equivalent four-pole network model based on distributed analog impedances and sources, which has a better modification of the one-dimensional photoacoustic cell.

According to the principle of electric circuit, the summation of the resistance R and the product of i ($\mathrm{i}=\sqrt{-1}$) and inductance ωL can be defined as the impedance Z_1 per unit length in units of kg/m^{4}s, i.e., $Z= R_a + \mathrm{i}\omega L_a$, and i times of capacitance ωC_a can be defined as the admittance Z_2 per unit length in units of m^{4}s/kg, i.e., $1/Z_2 = \mathrm{i}\omega C_a$.

The voltage $V(x)$ and current $I(x)$ in the transmission line equation can be used to describe the pressure amplitude and the flux of fluid of the photoacoustic cell, respectively. Hence, the voltage source of the equivalent four-pole network model, which describes the absorbed light source per unit length by measured gas, can be described as[14]:

$$U(x) = Z_2\{\bar{I}^0 - \beta[A\exp(\beta x/l) - B\exp(-\beta x/l)]\}, \quad (1)$$

where the current source is $I^0 = (\gamma-1)P\alpha/(\rho c^2)\ l/\pi$, and the propagation constant is $\beta=(Z_1/Z_2)^{1/2}$. A and B can be derived from $U_i(x)$ which can be obtained by iteration in computer. Finally propagation matrix of the result can be used to represent the photoacoustic process and properties of the whole photoacoustic system.

For the case of trace gas detection, the constants of acetylene at room temperature and atmospheric pressure are given in Tab.1, which shows the values of the parameters considered in the simulation for the photoacoustic cell by using equivalent four-pole network model. l_{res} represents the resonant length, d_{res} is the resonant diameter, l_{buf} is the buffer length, and d_{buf} is the buffer diameter. c is the velocity of sound, ρ is the density of the gas, C_p is the gas specific heat capacity at constant pressure per unit mass, $\gamma=C_p/C_v$ is the ratio of specific heat capacity at constant pressure and volume, μ is the viscosity of the gas, and κ is the thermal conductivity of the gas. By substituting these values into the MATLAB program, the photoacoustic responses versus resonance frequency and axial position of the photoacoustic cell are shown in Fig.1.

Tab.1 Simulation parameters

l_{res}	d_{res}	l_{buf}	d_{buf}	c
50 mm	5 mm	30 mm	14 mm	343 m/s
ρ	γ	C_p	μ	κ
1.11 kg/m^3	1.24	1460 J/kg·K	9.54×10^{-6} Pa·s	18.5 W/(m·K)

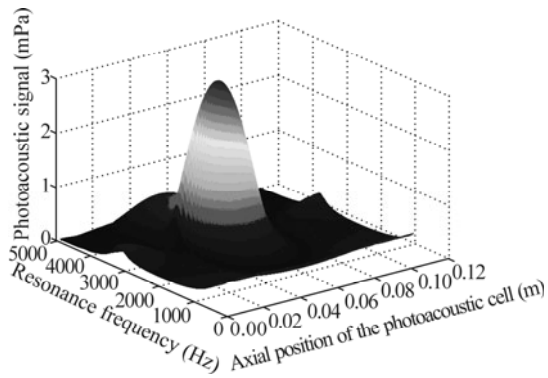

Fig.1 Photoacoustic signals at different frequencies and axial positions of the photoacoustic cell

Fig.1 shows that the maximum amplitude of the photoacoustic signal is obtained at the center which is the best position to locate a microphone. The absorption of acetylene (C_2H_2) increases at both ends due to the heating effects resulting from the laser beam passing through input and output windows.

Fig.2 shows that the photoacoustic signal is high at long length and wide diameter of the buffer. When the diameter of buffer decreases, the standing wave stretches out into the buffer cavities, which lowers the received photacoustic signal due to the position of the microphone is far.

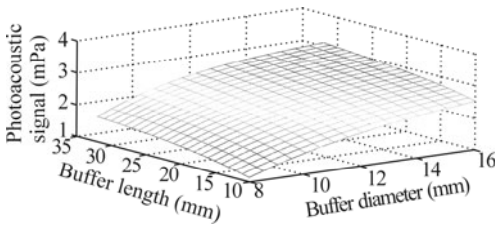

Fig.2 Photoacoustic amplitudes at different buffer lengths and diameters

Fig.3 shows the effects of buffer diameter and length on the photoacoustic signal and resonance frequency. We can observe from Fig.3(a) that an intersection occurs at the buffer length of about 25 mm. It can be noticed that before the length of diameter 25 mm, the resonance frequency increases with the decrease of the buffer diameter. Inversely, the frequency resonance decreases when buffer length is bigger than 25 mm. Due to the end correction $\Delta l \approx 0.6r$ (for open end), $f=c/(l+\Delta l)$[15], small diameter with short length of buffer produces high resonance frequency. The variation of resonance frequency is very

small with the buffer length of 25 mm. That is to say the buffer length of 25 mm has the minimum impact on resonance frequency.

Fig.3(b) shows that the PA signal is high at long length and wide diameter of the buffers. The optimal buffer length is at 25 mm, which is equal to a quarter of the acoustic wavelength ($\lambda/4$), i.e., $l_{res}=2l_{buf}$ ($l_{res} >> d_{res}$). In that case optimal background signal suppression is achieved. It is shown that the resonance frequency changes are almost constant and the amplitude of the photoacoustic signal is barely influenced when $d_{buf} \geqslant 3d_{res}$. Considering that oversize of photoacoustic cell needs more measuring gas and more material, the buffer diameter can be deduced to $d_{buf} \approx 3d_{res}$.

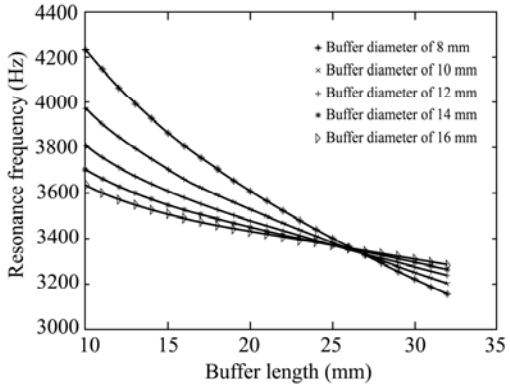

(a)

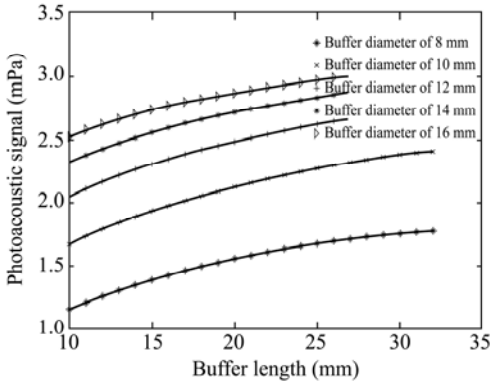

(b)

Fig.3 Effects of buffer diameter and length of the photoacoustic cell on (a) resonance frequency and (b) photoacoustic signal

The schematic diagram of experimental system for trace gas detection is illustrated in Fig.4. A single-mode distributed feedback (DFB) tunable diode laser (LC96AH74, Accelink Technology) operating at a wavelength of 1533 nm is used as the light source. Better sensitivity of photoacoustic detection is realized when the modulation frequency coincides with the acoustic resonant frequency depending on the resonator size. A temperature controller (TED200C, ThorsLabs) and a laser diode current controller (LDC250, ThorsLabs) are used to maintain output stability and control the modulation frequency of the laser. The photoacoustic cell made from stainless steel is used in the experiment with dumb-bell shape. A resonator connected between two buffers (made from aluminum) is served as the acoustic filter. Laser with input power of 10 mW is launched into a fiber collimator, and propagates along the axis of the photoacoustic cell which is with C_2H_2 concentration of 100 ppm. An electret microphone (WP-23502, Knowles Inc) is placed at the center of the cell to collect the acoustic signal which is then converted to voltage. The voltage is collected by a data acquisition system (DAQ), and finally is sent to a personal computer (PC) for analysis.

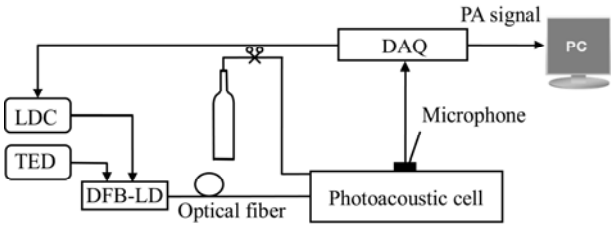

LDC: laser diode current controller; TED: temperature controller; DAQ: data acquisition system; PA: photoacoustic

Fig.4 Schematic diagram of the experimental system

Fig.5 shows the structure of the whole photoacoustic cell which is on an adjustable dovetail guide rail and supports the resonator cavity at the center. The buffer volumes are changed by using various inner diameters of aluminum ring. Each end of the resonant cell is fixed with an aluminum piston. By adjusting the relative location of the pistons, the buffer volume can be changed by increasing its length from 15 mm to 35 mm with step of 5 mm, while the diameters are varied by 2 mm from 8 mm to 16 mm. In the experiments, better photoacoustic response is achieved when the laser beam completely passes through the photoacoustic cell along the axis and the buffer must be sealed up with piston for air tightness.

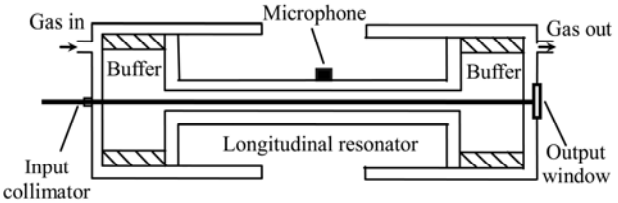

Fig.5 Structure of the photoacoustic cell

Buffers at both ends are varied in length by putting the piston lid slide along the length axis. From Fig.6, the minimum background signal appears when buffer length equals a quarter of acoustic wavelength ($\lambda/4$) of 25 mm, which is the optimal length for destructive interference of pressure amplitudes into the buffer. However in this case, the resonance frequency is not affected by the buffer

length too much.

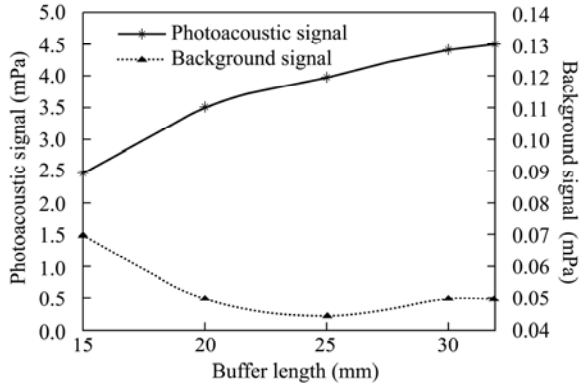

Fig.6 Experimental results of the photoacoustic signal and background signal for various buffer lengths with d_{res}=5 mm, l_{res}=50 mm and d_{buf} =16 mm

Fig.7 shows that the buffer diameter ranging from 8 mm to 12 mm increases the resonance frequency. At a certain diameter, buffers are close to the size of the resonator which is a longer one. Based on $f=c/2l_{res}$, the frequency is inversely proportional to the resonator length. Thus, the small buffer diameter has low resonance frequency. However, when the buffer diameter is larger than 14 mm, the resonance frequency is almost constant, as can be seen in the inset of Fig.7. It shows that the biggest deviation between experimental resonance frequency and simulation result appearing at the buffer diameter of 16 mm is 1.8%, while the smallest deviation is 0.46% at buffer diameter of 10 mm, thus the average deviation is 1.1%.

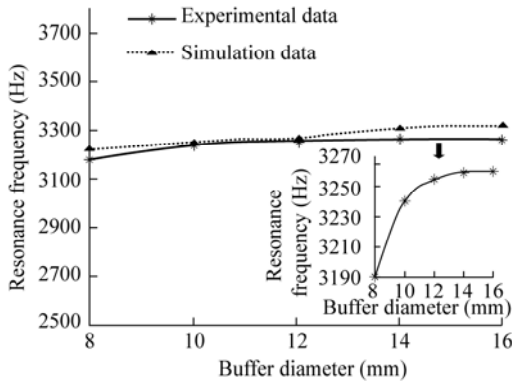

Fig.7 Experimental and simulation results of the resonance frequency with several buffer diameters under d_{res}=5 mm, l_{res}=50 mm and l_{buf}= 30 mm

According to Fig.8, the background signal is decreased when larger buffer diameter is applied whereas the photoacoustic signal is increased at the same time. In this case, the larger buffer diameter can obtain the higher photoacoustic signal which is good for the improvement of sensitivity. However, the oversize of photoacoustic cell needs more gas for measuring and more time to inflate, so the optimal size is practical for trace gas detection.

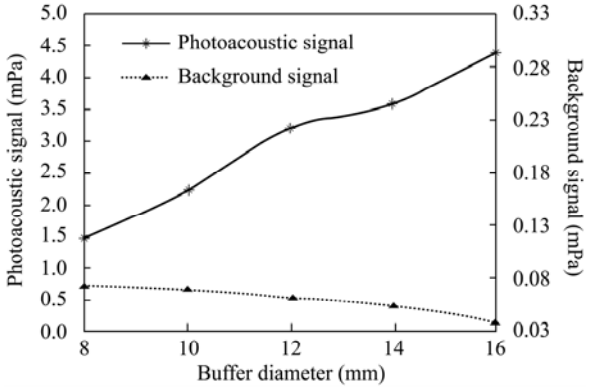

Fig.8 Effects of buffer diameter on the photoacoustic signal and background signal with d_{res}=5 mm, l_{res}=50 mm and l_{buf}=30 mm

Fig.9 depicts the experiment results which can match with the simulation analyses. The average deviation between experimental and simulation results is 1.1% with the buffer length of 30 mm, 0.46% with the buffer length of 25 mm, and 0.96% with the buffer length of 20 mm, respectively, due to imperfect seal of photoacoustic cell.

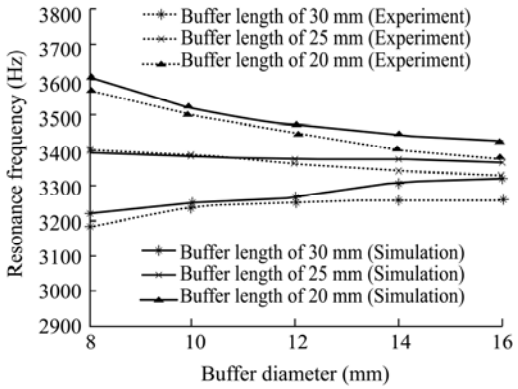

Fig.9 Comparison between experimental and simulation results for resonance frequency with different buffer diameters and lengths

A theoretic model is carried out to estimate the optimal buffer geometry. Based on the theoretic model analyses and the experiment results for buffer geometry of the photoacoustic cell, we can obviously see the influence of the buffer length and diameter on the photoacoustic signal, background signal and resonance frequency. Further investigation should be carried out to bring in the EDFA and the improvement of the circuit to test the minimum concentration of the gas.

Acknowledgement

The authors would like to thank Universiti Kebangsaan Malaysia (UKM) in providing Young Researcher Fellowship Grant 2012 for our visiting scholar.

References

[1] C. G. Teodoro, D. U. S. Schramm, M. S. Sthel, G. R. Lima, M. V. Rocha, J. R. Tavares and H. Vargas, Journal of Physics: Conference Series **214**, 012040 (2010).

[2] J. Laufer, C. Elwell, D. Delpy and P. Beard, Physics in Medicine and Biology **50**, 4409 (2005).

[3] W. Chen, B. Liu, H. Zhou, Y. Wang and C. Wang, European Transactions on Electrical Power **22**, 226 (2012).

[4] X. Chen, Q. M. Sui, F. Miao, L. Jia and J. Wang, Journal of Optoelectronics·Laser **22**, 1679 (2011). (in Chinese)

[5] W. L. Ye, X. Yu, C. T. Zheng, C. X. Zhao, M. L. Cong, Z. W. Song and Y. D. Wang, Optoelectronics Letters **7**, 217 (2011).

[6] M. Tavakoli, A. Tavakoli, M. Taheri and H. Saghafifar, Optics and Laser Technology **42**, 828 (2010).

[7] J. Kalkman and W. H. Van Kesteren, Applied Physics B: Lasers and Optics **90**, 197 (2008).

[8] L. C. Aamodt, J. C. Murphy and J. G. Parker, Journal of Applied Physics **48**, 927 (1977).

[9] S. Cristescu, D. C. Dumitras and D. C. A. Dutu, Proceedings of SPIE –The International Society for Optical Engineering **4068**, 261 (2000).

[10] F. G. C. Bijnen, J. Reuss and F. J. M. Harren, Review of Scientific Instruments **67**, 2914 (1996).

[11] Mohammed A. Gondal, Ahmed Asaad I. Khalil and Noura Al-Suliman, Applied Optics **51**, 23 (2012).

[12] M. Wolff, B. Kost and B. Baumann, International Journal of Thermophysics **33,** 1953 (2012).

[13] A. H. Benade, Journal of the Acoustical Society of America **44**, 616 (1968).

[14] S. Bernegger and M. W. Sigrist, Infrared Physics **30**, 375 (1990).

[15] Z. Bozoki, A. Miklos and P. Hess, Review of Scientific Instruments **72**, 1937 (2001).